Accelerators, Beamlines, Experimental Apparatus, and Experimental Techniques

Beamlines

Absolute flux measurements for IR spectromicroscopy
Martin, M.C., K. Knutsen, W.R. McKinney

Beamline 9.3.1: Monochromator upgrade
Schlachter, A.S., R. Weidenbach, E. Domning, W. Steele, T. Miller, C. Hernikl, T. Warwick

Coherent far IR bursts measured at BL 1.4.2
Martin, M.C., J. Byrd, F. Sannibale, W.R. McKinney

Femtosecond synchrotron pulses from the Advanced Light Source
Schoenlein, R.W., A. Cavalleri, H.H.W. Chong, T.E. Glover, P.A. Heimann, C.V. Shank, A.A. Zholents, M.S. Zolotorev

Giant terahertz power levels from relativistic electrons
Carr, G.L., M.C. Martin, W.R. McKinney, K. Jordan, G.R. Neil, G.P. Williams

New IR microscope and bench installed at BL 1.4
Martin, M.C., H.-Y. Holman, W.R. McKinney

Status of the 5.3.2 bend magnet polymer STXM
Kilcoyne, D., H. Ade, T. Tyliszczak, A.P. Hitchcock, E.G. Rightor, G.E. Mitchell, M. Kritscher, T. Warwick, K. Franck, E. Anderson

Status report on Beamline 10.3.2
Marcus, M.

Suite of three protein crystallography beamlines with single superconducting bend magnet as the source
MacDowell, A.A., D. Cambie, D. Plate, R. Duarte, N. Kelez, H.A. Padmore, M. Howells, R. Celestre, E. Domning, J. Holton, C. Cork, T. Earnest, J. Dickert, G. Meigs, J. Krupnick, T. Alber, S. Berger

The use of micro-FTIR to characterize soil minerals and boron adsorption
Pittiglio, S., H.E. Doner

Absolute Flux Measurements for IR Spectromicroscopy

Michael C. Martin[a], Kelly Knutsen[b] Wayne R. McKinney[a]
[a] Advanced Light Source Division, Lawrence Berkeley National Laboratory, Berkeley, CA 94720
[b] Dept. of Chemistry, University of California, Berkeley, CA 94720

1. INTRODUCTION

Measurements of the effects of exposure to IR light at the spectromicroscope at beamline 1.4.3 has necessitated an estimate of the absolute flux levels in the IR optical bench and in the microscope. We calculated the IR flux levels from both a thermal source and the ALS, and compared them to measurements taken at the beamline. We find a self consistent picture which can be used to estimate the absolute exposure to cells and bacteria which are examined in the IR microscope.

2. EXPERIMENTAL

The thermal ("globar") source in the Nicolet 760 IR bench was measured with a disappearing filament style optical pyrometer to have a brightness temperature of ~1343K. This allowed us to calculate the "greybody power" emitted by the filament, using the emissivity of tungsten. We also measured the output of the thermal source with a Molectron PowerMax 500D with a 19 mm dia. PM10V1 detector. To measure ratios of light both before and after the bench and the microscope a more sensitive mid IR detector was needed so we employed a T3-09 9mm dia. energy detector, and a 200 Hz chopper. We also calculated the power of the synchrotron beam using the standard bending magnet formulae. The table below summarizes our results. Unless enumerated otherwise the numbers are in watts. Bold numbers are experimental data, others are calculations or estimates.

Greybody power	1.70E-04	**0.0479**	Synchrotron Power	3.73E-02
1 to 20 microns			1 to 20 microns	
1 mm^2, 0.0064 str, 1343 K			10 x 40 mr, 1.9 GeV, 4.81 m	
Real emitting area, mm^2	100	1	Beamline coupling loss	0.333
			20 out of 40 mr * 0.67 diamond	
Bench efficiency	0.372	0.372	Bench efficiency	0.372
Chopped Energy Detector			Chopped Energy Detector	
15.9/42.7			**15.9/42.7**	
Microscope Vignetting	0.1677	0.1677	Microscope Vignetting	1
Chopped Energy Detector				
1.5/15.9 * 12^2/9^2				
Microscope efficiency	0.225	0.225	Microscope efficiency	0.225
0.6/(1.5*12^2/9^2)			**0.6/(1.5*12^2/9^2)**	
Chopped Energy Detector			Chopped Energy Detector	
Power at sample	2.39E-04	6.72E-04	Power at Sample	1.04E-03
Greybody			Synchrotron	
Ratio of Synch/Greybody	**2**		Peak Power at Sample	5.20E-02
by MCT in Microscope			Synchrotron (*50)	
Ratio from this work	1.55		for 2ns/40ps	

3. RESULTS AND DISCUSSION

Starting from two calculations, and one measurement the table precedes from top to bottom from the two sources, thermal and synchrotron to the sample. At each step, there were many factors to consider. For example, the long depth of field of the synchrotron source means that all 40 horizontal mr of beam is not coupled into the microscope, and the synchrotron beam has a diamond window loss which the thermal beam does not. Moreover, the synchrotron beam has been carefully moved from the center of the optical axis so that it is not vignetted by the special coating in the center of the beam splitter in the optical bench, and the microscope optics have been adjusted to optimally transmit the synchrotron beam. This requires that the vignetting ratios for the two cases be different. We have done our best to honestly estimate the various factors, and measure them where feasible without significant disassembly of the beamline optics.

The final results are satisfying in that the ratio of the total synchrotron to thermal flux (1.55) that we get from our careful combination of theoretical and experimental measurements matches well within the error of our methods the ratio (2.0) we measure by comparing the two sources directly with the LN_2-cooled MCT detector in the microscope. The brightness advantage of the synchrotron (>100) is also verified. The overall error in the estimates is well represented by the factor of 2.8 between the two methods for estimating the power of the thermal source. The continuous power at the microscope integrated from 400 to 10000 cm^{-1} is estimated to be approximately 1 mW, and the peak power at the top of an ALS pulse to be fifty times (2 nsec / 40 psec) that, or 50 mW.

ACKNOWLEDGEMENTS

This work was performed with support by the Directors, Office of Energy Research, and Basic Energy Sciences, Materials Science Division, of the United States Department of Energy under Contract No. DE-AC03-76SF00098.

REFERENCES

1. Michael C. Martin, Nelly M. Tsvetkova, John H. Crowe, and Wayne R. McKinney, "Negligible sample heating from synchrotron infrared beam," Applied Spectroscopy, **55**(2), 111-113 (2001).

2. Hoi-Ying N. Holman, Michael C. Martin, Eleanor A. Blakely, Kathy Bjornstad, and Wayne R. McKinney, "IR spectroscopic characteristics of cell cycle and cell death probed by synchrotron radiation based Fourier transform IR spectromicroscopy," Biopolymers (Biospectroscopy), **57**[6], 329-335 (2000).

3. Hoi-Ying N. Holman, Kathleen A. Bjornstad, Morgan P. McNamara, Michael C. Martin, Wayne R. McKinney, and Eleanor A. Blakely, "Synchrotron Infrared Spectromicroscopy as a Novel Bioanalytical Microprobe for Individual Living Cells: Cytotoxicity Considerations," Journal of Biomedical Optics 2002, *In Press.*

Principal investigator: Michael C. Martin, Advanced Light Source Division, LBNL, 510-495-2231, MCMartin@lbl.gov

Beamline 9.3.1:
Monochromator Upgrade

Fred Schlachter, Richard Weidenbach, Ed Domning, William Steele, Tom Miller,
Chris Hernikl, and Tony Warwick[1]
[1]Advanced Light Source, Ernest Orlando Lawrence Berkeley National Laboratory,
University of California, Berkeley, California 94720, USA

INTRODUCTION

A double-crystal monochromator is installed on bend-magnet beamline 9.3.1. It is designed to provide photons in the energy range 2.3 to 5.5 keV. Although it has successfully operated for energy scans over limited energy ranges, it has generally not been used for applications requiring scans over a large energy range, e.g., for EXAFS. The monochromator has been redesigned and rebuilt for improved performance. The upgraded monochromator shows improved thermal and mechanical stability, and energy scans over large energy ranges are now possible. A new control system and user interface are being implemented. The beamline is now ready for users.

ISSUES

The performance of the monochromator as designed was limited by several factors.

- thermal stability due to insufficient cooling of the first crystal;
- mechanical stability of the crystal mounts;
- lack of position readouts of crystal adjustments;
- outdated and undocumented control system.

The primary limitation of the monochromator is that the first crystal absorbs significant heat, resulting in thermal expansion and an increase of d-spacing of the crystal. This effect, before cooling was implemented, was time and photon-energy dependent, and limited both scanning range and stability of beam position and intensity with time. A second limitation was mechanical stability of the crystal mounts, and coupling of crystal motions (theta and chi angles). Picomotors were used to control theta and chi adjustments inside the vacuum, but, without position readouts, it was easy to get lost, resulting in tuning difficulties and unforgiving operation. Finally, the control system was essentially non-commercial and undocumented, and the LabView code was not documented, resulting of difficulties in upgrading the equipment and/or the operating system.

IMPROVEMENTS

The ground rule for upgrading the monochromator was to preserve the mechanical linkage (the "boomerang") which controls the position and angle of the two crystals in the monochromator.

The crystal mounts were totally re-engineered. The primary improvement was to add water cooling to the first crystal. This was achieved by circulating chilled temperature-controlled water

through a copper plate which is part of the mount for the first crystal. Indium foil and a gallium eutectic are the heat-transfer media to cool the first crystal.

The support arrangement for each rotation axis of the crystal mounts was changed from a single flexural hinge to a pair of flexural hinges, providing considerably improved mechanical stability and isolation of theta and chi motions.

Theta and chi coarse adjustments are made, as before, by picomotors in vacuum. However, a piezo actuator has been added in series with the picomotor for adjustment of theta (theta puts the second crystal on the Bragg peak of the first crystal) for eventual feedback on either photon beam intensity or vertical beam position (which are coupled). Provision has been made for installing a piezo actuator for adjustment of chi (left-right tilt adjustment of the second crystal) should fine adjustment and/or feedback on horizontal beam position be required.

LVDTs (Linear Variable Differential Transformers) were installed to measure theta and chi position. These allow computer control of theta and chi, feedback, and maintaining reference positions. The beamline is now easy to tune and control.

The LabView code running the control and data-acquisition systems has been entirely rewritten, keeping the flavor of the previous code while adding new features, making operation of the beamline more user friendly, and having a maintainable code. New counting cards add additional counting channels.

Many improvements were made to mechanical parts of the boomerang and crystal mounts, primarily in the selection of materials to provide smooth long-term operation and to minimize galling and other maintenance issues. The rotary parts of the mechanisms were redesigned and rebuilt as needed.

OPERATION and TESTING

Energy repeatability is of concern to users when multiple scans are made over the same energy range. The method used previously was to remove backlash from the mechanism by selecting a low energy, then increasing the energy to the starting point of the scan. Motor steps were counted to determine energy. A tilt sensor was used to “home” the motor from time to time. We found that motor steps are not a reliable method for determining photon energy. For example, a series of measurements of photoabsorption in argon gas had the peak spread over greater than 1 eV, with a mean spread of nearly 0.4 eV. The tilt sensor, previously used for homing only, was at least a factor of two better (see Fig. 1). We are thus using the tilt sensor to measure photon energy, pending installation of a rotary encoder for installation on the rotation axis of the first crystal. This will provide improved energy repeatability.

Tests are underway on beam size and beam-position stability. Initial results show a beam of less than 1-mm diameter, with beam position stability of +/- two mm in scans over a range of 2000 eV. Flux is relatively constant in scans over a large energy range (see Fig. 2).

Energy calibration has been accomplished using photoabsorption and photoemission measurements.

The new user interface is integrated with the new control system, and is presently undergoing testing. It is being phased in as new functions become available.

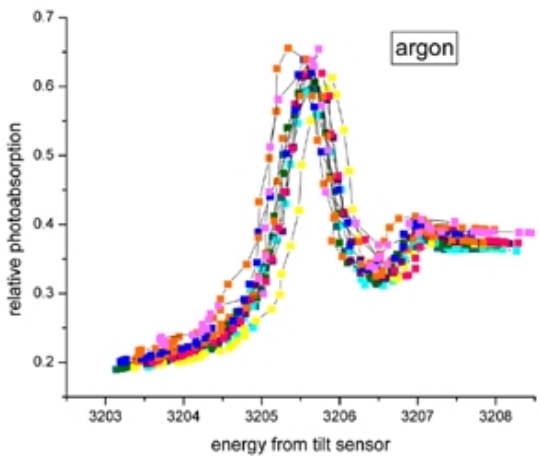

Figure 1. Relative photoabsorption in argon gas as a function of photon energy (eV) as measured by the tilt sensor. Multiple scans are shown to indicate repeatability.

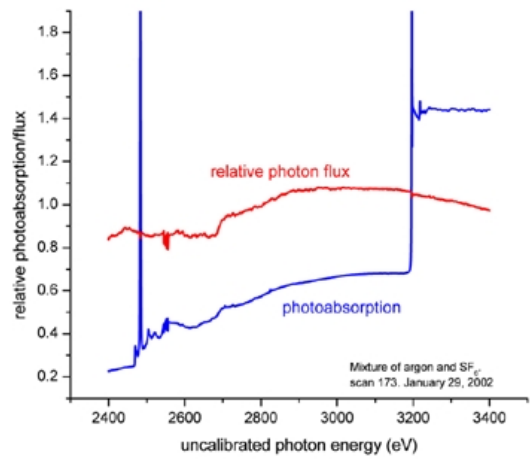

Figure 2. Relative photoabsorption and photon flux for a mixture of argon and SF_6 gases. Scan was made continuously with no adjustments.

OUTLOOK

We expect beamline 9.3.1 to operate with greatly improved stability and ease, and greater scanning range than was previously possible. It is a very useful beamline for K-shell studies on elements from sulfur through vanadium, and for L-shell and M-shell work on elements with electron binding energies in the range 2300 to 5500 eV.

ACKNOWLEDGMENTS

We thank Alastair MacDowell, Dennis Lindle, Will Thur, and Wayne Stolte for their kind assistance to this project.

This work was supported by the Director, Office of Energy Research, Office of Basic Energy Sciences, Materials Science Division, of the U.S. Department of Energy under Contract No. DE-AC03-76SF00098.

Principal investigator: Fred Schlachter, Advanced Light Source, Ernest Orlando Lawrence Berkeley National Laboratory. Email: fsschlachter@lbl.gov. Telephone: 510-486-4892.

Coherent Far IR Bursts Measured at BL 1.4.2

Michael C. Martin, John Byrd, Fernando Sannibale, and Wayne R. McKinney
Advanced Light Source, Lawrence Berkeley National Laboratory
University of California, Berkeley, California 94720, USA

INTRODUCTION

We have performed the first measurements at the ALS of coherent far-IR bursts coming from instabilities within a high-current single electron bunch.

The 2-bunch mode operations of the ALS afforded us the opportunity to use the machine while it was tuned for high currents in individual electron bunches. We have used a number of accelerator physics shifts to make measurements with well-controlled setups as well as additional measurements during normal 2-bunch operations. Recent investigations at other light sources [1-6] have observed far-IR bursting at high bunch currents. We want to investigate these bursts more carefully towards the goal of understanding how to make use of high-intensity coherent far-IR synchrotron light as a new source of far-IR that is many orders of magnitude brighter than the best presently available sources.

TIME DOMAIN MEASUREMENTS

As an initial investigation into coherent far-infrared synchrotron radiation we placed a liquid He cooled Silicon Bolometer with integrated pre-amplifiers just outside a 20 mm diameter diamond window mounted in the 'switchyard' at Beamline 1.4. A single extra mirror was inserted in the switchyard to direct the collimated beam through this window into the bolometer without disturbing the alignment of the IR beamlines. A digitizing oscilloscope recorded the output of the detector. We observed large intensity bursts when the single bunch current was very high. Fig. 1 shows time traces of the bolometer output voltage for three different beam currents in single bunch operation. Although the bursts seemed to be quasi-random, at certain currents the bursts occurred within a periodic envelope, as evidenced by the middle trace in Fig. 1. The rise and fall times of the bursts were detector limited, therefore the damping mechanism may not be inferred immediately. The single bunch current threshold for the onset of

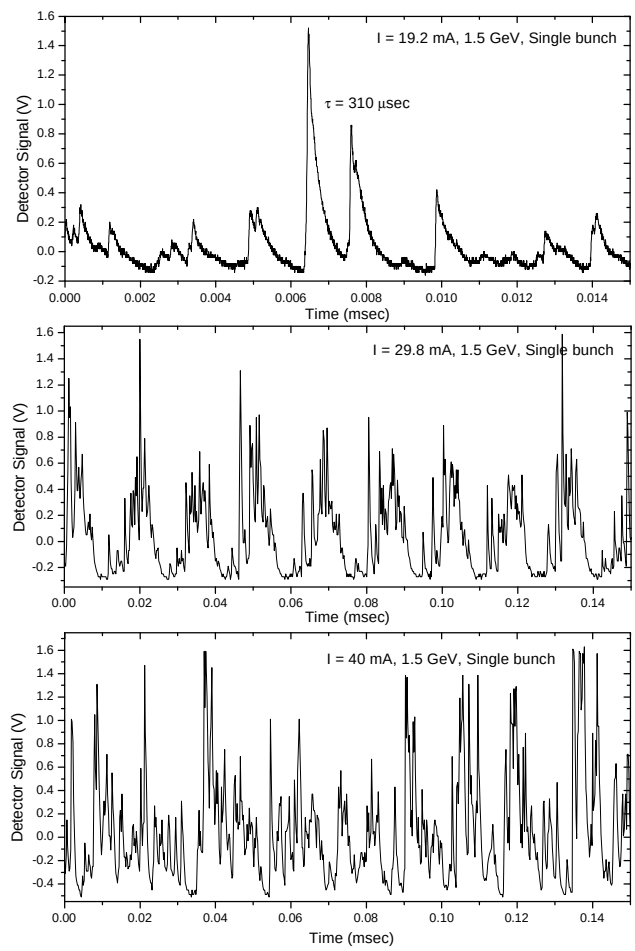

Figure 1. Far-IR detector signal vs time for three different beam currents. Note the expanded time scale for the top panel.

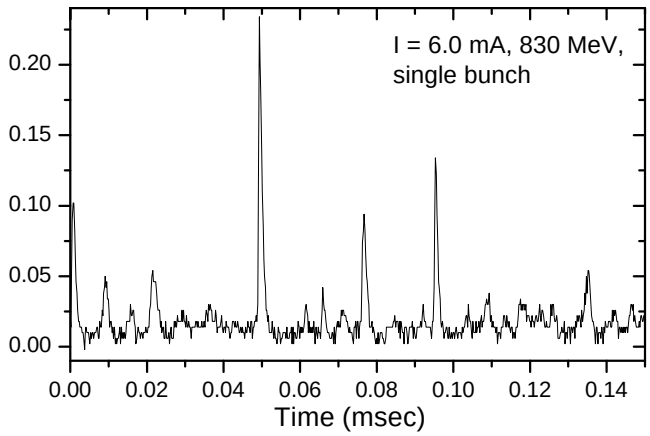

Figure 2. Bursting observed at 830 MeV which shows a quite different time envelope.

bursts is approximately 7 mA at 1.5 GeV. The transition to bunching of the bursts within a super period occurs at about 27 mA at 1.5 GeV.

Since the bursts seem to be related to high peak currents within a bunch, reducing the RF power will lengthen the bunch and therefore cause the bursts to stop. At 14 mA and 1.9 GeV, the bursts go away by reducing the RF power from 120 to 90 KW; returning to 120 KW causes the bursts to reappear. At 1.5 GeV and 14 mA, the bursts can be stopped by dropping the RF power from 120 to 1.5 KW.

A measurement of the bursting at 830 MeV electron energy at 6 mA single bunch current showed distinctly different time behavior as shown in Fig. 2.

SPECTRAL MEASUREMENTS

By using a combination of filters with the above setup we determined the spectral content of the bursts was below 100 cm^{-1} (wavelengths longer than 100 microns). To make this more quantitative, we used the Bruker 66v/S FTIR spectrometer on BL 1.4.2 to measure the bursts that occur at the very top of the fill during regular 2-bunch mode operations. By quickly averaging 100 interferograms over 50 seconds we integrated long enough to demonstrate the average spectral content of the bursts. Shown in Fig. 3 is the measured intensity of the bursts as a function of wavelength, ratioed to the incoherent synchrotron signal measured at low beam current. The bursts are peaked at ~27 cm^{-1}. This indicates a microbunching within the electron bunch having a period on the order of 400 microns (or approximately 30 times smaller than the normal ALS bunch length). The bursting was clearly dependent on the beam energy, with higher intensity at 1.5 GeV. This is to be expected, as the bunch length is proportional to $E^{3/2}$, implying higher peak currents at 1.5 GeV than 1.9 GeV, and therefore a greater tendency for instabilities and hence microbunching. Overall, the burst intensity dropped with decreasing beam current, with the spectral content remaining essentially unchanged.

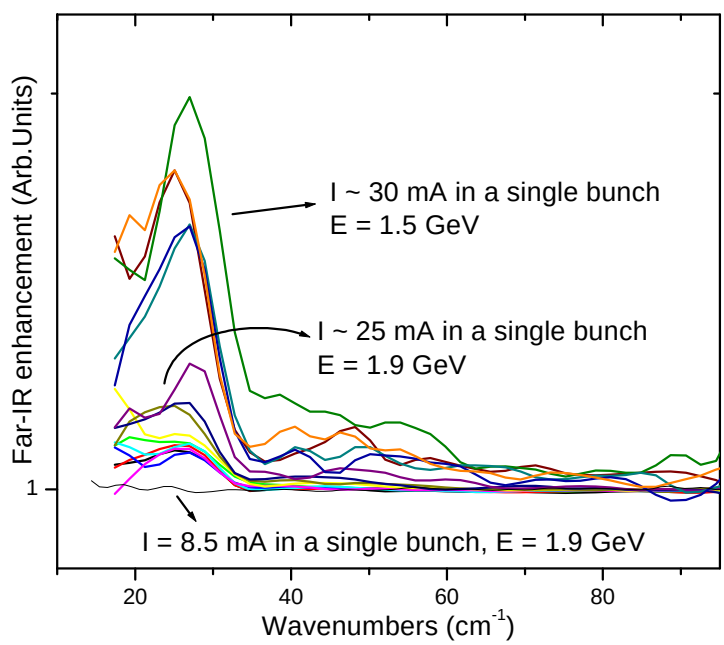

Figure 3. Spectrum of coherent far-IR bursts measured at Bl1.4.2 as the current was decaying.

We are continuing these measurements to gain a greater understanding into coherent synchrotron emission both

from instabilities (as measured here) and hopefully in a stable manner. In the near future, we will make additional measurements using femtosecond sliced electron bunches (in collaboration with the femtosecond x-ray team at LBNL) which will allow a clean study of coherent emission from a well known transient short bunch. Because this will be a laser pumped measurement with synchronized optical detection, electron beam instabilities and oscillations will not be a factor. We have also collaborated with researchers at Brookhaven National Laboratory and Thomas Jefferson National Laboratory to measure the coherent far-IR emitted from a bend magnet in their energy-recovery linear accelerator based infrared free electron laser [7] (reported in a separate compendium abstract).

REFERENCES

1. H. Tamada and H. Tsutsui, *Nuclear Instr. & Meth*. **A331**, 566 (1993).
2. A. Andersson, M. S. Johnson and B. Nelander, *Optical Engineering*, **39**, 3099 (2000)
3. U. Arp, G.T. Fraser, A.R. Hight Walker, T.B. Lucatorto, K.K. Lehmann, K. Harkay, N. Sereno and K.-J. Kim, *Phys. Rev. Special Topics, Accelerators and Beams* **4**, 54401 (2001)
4. G.L.Carr, S.L.Kramer, J.B.Murphy, R.P.S.M.Lobo and D.B.Tanner, Nucl. Instr. & Meth. A463, 387 (2001).
5. M. Abo-Bakr, J. Feikes, K. Holldack, G. Wüstefeld and H.-W. Hübers, to be published.
6. D. X. Wang, G. A. Krafft, and C. K. Sinclair, Phys. Rev. E, 57, 2283 (1998).
7. G.L. Carr, M.C. Martin, W.R. McKinney, K. Jordan, G.R. Neil, and G.P. Williams, to be published.

This work was supported by the Laboratory Directed Research and Development Program of Lawrence Berkeley National Laboratory under the Department of Energy Contract No. DE-AC03-76SF00098.

Principal investigator: Michael C. Martin, Advanced Light Source Division, Lawrence Berkeley National Laboratory. Email: MCMartin@lbl.gov. Telephone: 510-495-2231.

Femtosecond Synchrotron Pulses from the Advanced Light Source

R.W. Schoenlein[1], A. Cavalleri[1], H.H.W. Chong[1,2], T.E. Glover[3], P.A. Heimann[3], C.V. Shank[1,2], A.A. Zholents[4], M.S. Zolotorev[4]

[1]Materials Sciences Division, Ernest Orlando Lawrence Berkeley National Laboratory, University of California, Berkeley, California 94720, USA
[2]University of California Berkeley, Berkeley, California 94720, USA
[3]Advanced Light Source, Ernest Orlando Lawrence Berkeley National Laboratory, University of California, Berkeley, California 94720, USA
[4]Accelerator and Fusion Research Division, Ernest Orlando Lawrence Berkeley National Laboratory, University of California, Berkeley, California 94720, USA

An important new area of scientific research in chemistry, physics, and biology is the investigation of ultrafast structural dynamics in condensed matter using femtosecond x-ray pulses. The dynamic properties of materials are governed by atomic motion which occurs on the fundamental time scale of a vibrational period, ~100 fs. This is the time scale of interest for ultrafast chemical reactions, non-equilibrium phase transitions, vibrational energy transfer, surface desorption and reconstruction, and coherent phonon dynamics. To date, our understanding of these processes has been limited by lack of appropriate tools for probing the atomic structure on an ultrafast time scale. X-ray techniques such as diffraction and EXAFS yield detailed information about "static" atomic structure. However, the time resolution of high-brightness synchrotron x-ray sources such as the Advanced Light Source (~30 ps) is nearly three orders of magnitude too slow to directly observe fundamental atomic motion. Conversely, femtosecond lasers measure transient changes in optical properties of materials on a 10 fs time scale, but optical properties are only indirect indicators of atomic structure.

We have recently demonstrated a novel scheme for generating ultrashort pulses of synchrotron radiation[1]. Our approach is to create femtosecond time-structure on a long electron bunch by using a femtosecond laser pulse to modulate the energy of an ultrashort slice of the bunch. The modulation is achieved via interaction between the electrons and the light field in a wiggler (Figure 1a). Half of the electrons overlapping with the ultrashort pulse are accelerated and half are decelerated depending on the optical phase. The laser-induced energy modulation is several times larger than the rms beam energy spread at the ALS (~1.8 MeV), and only an ultrashort slice of the electron bunch experiences this modulation. The accelerated and decelerated electrons are then spatially separated from the rest of the electron bunch (in a dispersive bend of the storage ring) by a transverse distance that is several times larger than the rms transverse size of the electron beam (Figure 1b). Finally, by imaging the displaced beam slice to the experimental area, and by placing an aperture radially offset from the focus of the beam core, we will be able to separate out the radiation from the offset electrons (Figure 1c).

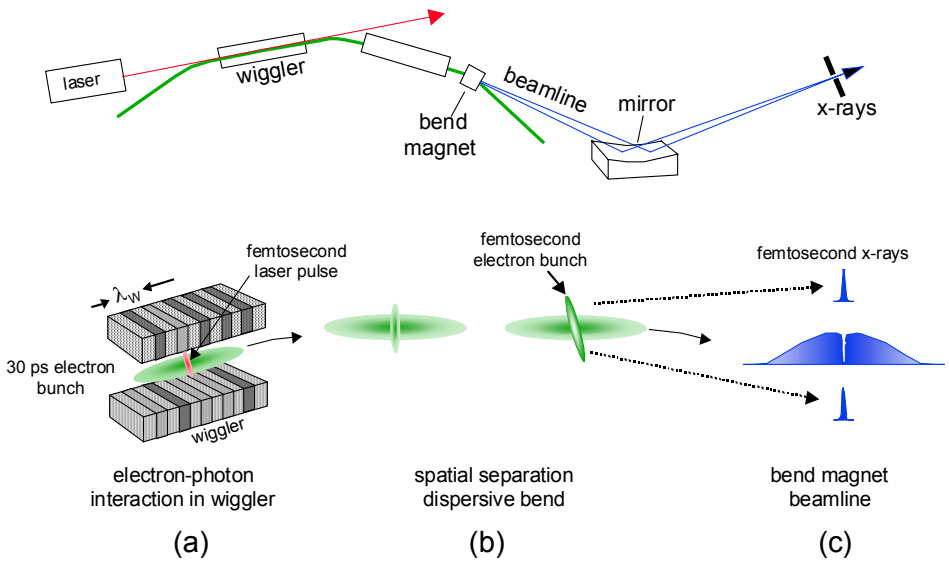

Figure 1. Schematic illustration of the technique for generating femtosecond synchrotron pulses. (a) laser/electron beam interaction in resonantly-tuned wiggler, (b) separation of accelerated femtosecond electron slice in a dispersive (bend) section, (c) generation of femtosecond x-rays at a band-magnet beamline.

This technique has recently been implemented on ALS beamline 5.3.1. A cryogenically cooled Ti:sapphire femtosecond laser system is located near the beamline endstation, and the laser pulses (~1 mJ, 100 fs pulse duration, 2 kHz repetition rate) are projected across the storage ring roof blocks to sector 5, where they enter the main vacuum chamber through a back-tangent optical port. Amplified femtosecond pulses co-propagate with the electron beam through wiggler W16 in sector 5. A photon stop/mirror following the wiggler reflects the laser light and the visible wiggler emission out of the vacuum chamber for diagnostic purposes in order to verify the spatial, spectral, and temporal overlap of the laser beam with the fundamental (undulator-like) emission from the wiggler.

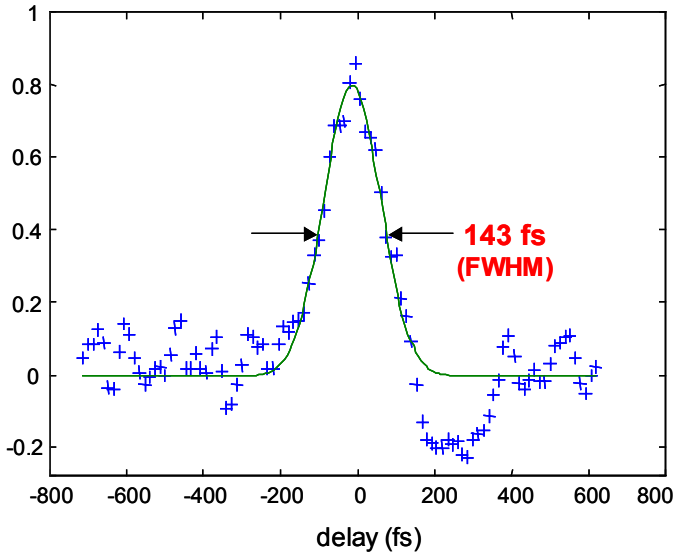

Figure 2. Cross correlation of an ultrashort synchrotron pulse with femtosecond laser pulse. The deconcolved synchrotron pulse duration is 143 fs (FWHM).

Femtosecond duration synchrotron pulses are directly measured by cross-correlating the visible light from bend-magnet beamline 5.3.1 at the ALS with a delayed laser pulse in the nonlinear crystal, BBO. Figure 2 shows a laser synchrotron cross-correlation measurement corresponding to synchrotron pulses of <150 fs duration, the shortest pulses ever generated from a synchrotron. Additionally, these measurements were made during normal multi-bunch operation of the storage ring, which illustrates the compatibility of this approach with the requirements of other synchrotron users, notably the protein crystallography beamline which simultaneously uses the wiggler W16. An important point is that the femtosecond time structure will be invariant over the entire spectral range of bend-magnet emission from the near infrared to the x-ray regime, making this a very powerful tool for femtosecond spectroscopy.

REFERENCES

[1] A.A. Zholents, M.S. Zolotorev, *Phys. Rev. Lett.* **76**, (1996) 912.

[2] R.W. Schoenlein, S. Chattopadhyay, H.H.W. Chong, T.E. Glover, P.A. Heimann, C.V. Shank, A. Zholents, and M. Zolotorev, *Science*, **287**, (2000), 2237.

[3] R.W. Schoenlein, S. Chattopadhyay, H.H.W. Chong, T.E. Glover, P.A. Heimann, C.V. Shank, A. Zholents, and M. Zolotorev, *Appl. Phys. B*, **71**, (2000), 1.

ACKNOWLEDGMENTS

This work was supported by the Director, Office of Science, Office of Basic Energy Sciences of the U.S. Department of Energy under Contract No. DE-AC03-76SF00098

CONTACT

Principal investigator: Robert Schoenlein, Materials Sciences Division, Ernest Orlando Lawrence Berkeley National Laboratory. Email: rwschoenlein@lbl.gov. Telephone: 510-486-6557.

Giant Terahertz Power Levels from Relativistic Electrons

G.L. Carr,[1] Michael C. Martin,[2] Wayne R. McKinney,[2]
K. Jordan,[3] George R. Neil,[3] and G.P. Williams[3]
[1]National Synchrotron Light Source, Brookhaven National Laboratory, Upton, NY 11973,
[2]Advanced Light Source, Lawrence Berkeley National Laboratory, Berkeley, CA 94720,
[3]Free Electron Laser, Jefferson Lab, 12000 Jefferson Avenue, Newport News, VA 23606

INTRODUCTION

We present measurements of both power and spectral content that confirm theoretical predictions of the generation of 20 watts (average) of broadband THz radiation pulses. The experiments were performed using the energy recovery linac (ERL) at the Jefferson Lab Free Electron Laser (JLab FEL)[1]. This facility offers a combination of very short electron bunches (~ 500 fs), relatively high average beam current (up to 5 ma), and up to a 75 MHz repetition rate.

The THz region, (1 THz = 33 cm^{-1} or 4 meV), lies in the far infrared spectral range where conventional thermal sources are very weak. A significant advancement in broadband THz sources has occurred over the past decade with the advent of coherent THz radiation emission from photocarriers in a biased semiconductor[5]. An energy per pulse of about 1μJ has been achieved, implying MW peak powers, but at repetition rates of 1 kHz such that average power levels are only 1 mW[5].

The present work describes a different process for producing coherent THz radiation by accelerated electrons. As schematically shown in Figure 1, electrons are photoemitted from GaAs, brought to relativistic energies (~ 25 MeV) in a linac and then transversely accelerated by a magnetic field to produce the desired THz emission as synchrotron radiation. If the electron bunch dimensions are small (in particular, the bunch length is less than the wavelength of observation), one obtains a multiparticle coherent enhancement[6,7].

Conceptually it is easy to understand the many orders of magnitude gain realized in these experiments by making a comparison with a more conventional (non-relativistic) THz source. We can compare the power produced per electron, and use Larmor's formula[19] for the radiated power. In CGS units it takes the form:

$$Power = \frac{2e^2a^2}{3c^3}g^4$$

where e is the charge, a is the acceleration, c the speed of light and γ is the ratio of the mass of the electron to its rest mass. In case A (the conventional THz emitter), these carriers immediately experience a force from the bias field (~100 volts across a 100 micron gap) of ~10^6 V/m, which results in an acceleration of

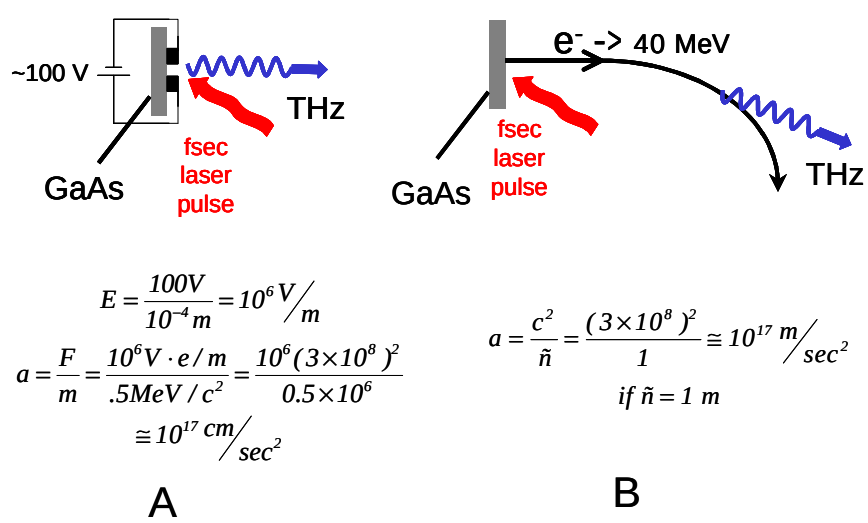

Fig. 1. Comparison between coherent THz radiation generated by a conventional laser-driven THz source (A) and the relativistic source described here (B).

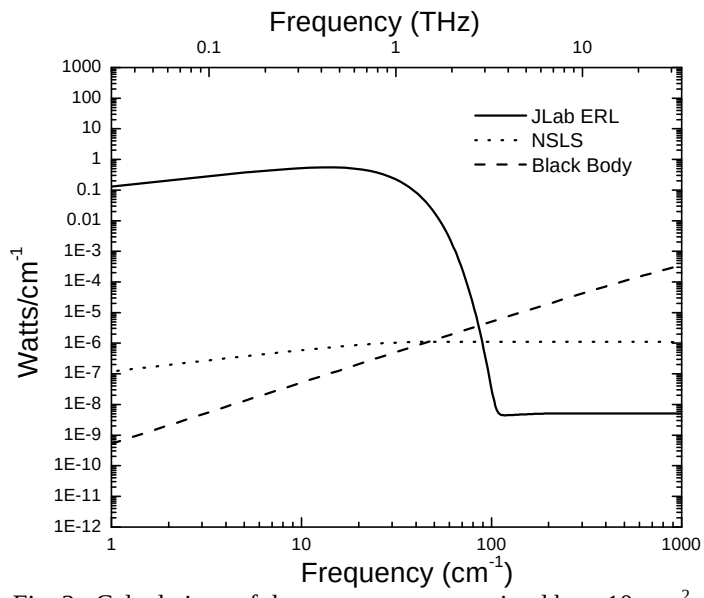

Fig. 2. Calculations of the average power emitted by a 10 mm^2 2000 K thermal source (dashed), the NSLS VUV ring at BNL (dotted), and the JLab ERL (solid).

10^{17} m/s^2. The entire process is completed in less than 1 ps, resulting in spectral content up to a few THz. In case B, the same number of charge carriers are brought to a relativistic energy of > 10 MeV in a linac, after which a magnetic field bends their path into a circle of radius $r = 1$m resulting in an acceleration $c^2/r = 10^{17}$ m/sec^2, the same as for case A. An observer for case B also detects a brief pulse of electromagnetic radiation as an electron bunch passes by. The bunch length determines the spectral range over which the coherent enhancement occurs. For an electron energy of 10 MeV ($\gamma = 21$), and with $r = 1$ m, we obtain a dt of about 500 fs, which is comparable to the bunch length. The resulting spectral content extends up to about 1 THz, the same spectral range as for case A. Thus, assuming the same number of electrons, the ratio of the power radiated by the conventional THz generation to the present generation is given by $\gamma^4 = 2 \times 10^5$, with $\gamma = 21$. In practice, the electron energy can be significantly larger, but this simply adds relatively weak (incoherent) intensity at higher frequencies and leaves the low frequency (THz) intensity essentially unchanged.

The results of calculations of the radiation for a conventionally synchrotron, a thermal IR source, and the JLab source are shown in Fig. 2 in units of (average) W/cm^{-1} over the range 1-1,000 cm^{-1}, or 0.03 to 33 THz. The superiority of the JLab ERL in the THz range is clear.

EXPERIMENTAL RESULTS AND DISCUSSION

In our experiments, the electrons were generated using the frequency doubled (530 nm) output of a Coherent Antares model Nd:YLF laser operating at sub-multiples of frequencies up to 74.8 MHz, and with an average power of a few watts incident on a Cs coated GaAs cathode. The resulting photoelectrons were accelerated using a DC voltage of 300 kV into a superconducting linac and accelerated to energies of up to 40 MeV.

The THz radiation was extracted from a dipole magnet of 1 m bending radius immediately prior to the free-electron laser cavity, the latter being unimportant for these experiments. For the total power measurements the light exited the accelerator vacuum chamber through a 10 mm aperture diamond window subtending an angle of 20 × 20 mrad relative to the source point. The emerging beam was focused onto a calibrated pyroelectric detector, with which the total power was measured, and which confirmed the predictions of the calculations for this aperture, charge per bunch and repetition.

The spectral content of the emitted THz light was analyzed using a Nicolet 670 rapid-scan Michelson interferometer with a silicon beamsplitter and a 4.2K Infrared Laboratories bolometer. The diamond window on the accelerator was replaced by a larger crystal quartz window to increase the light collection to 60 × 60 mrad. An 80 cm focal length spherical mirror produced a 48 mm diameter collimated beam compatible with the Nicolet 670 interferometer optics. A

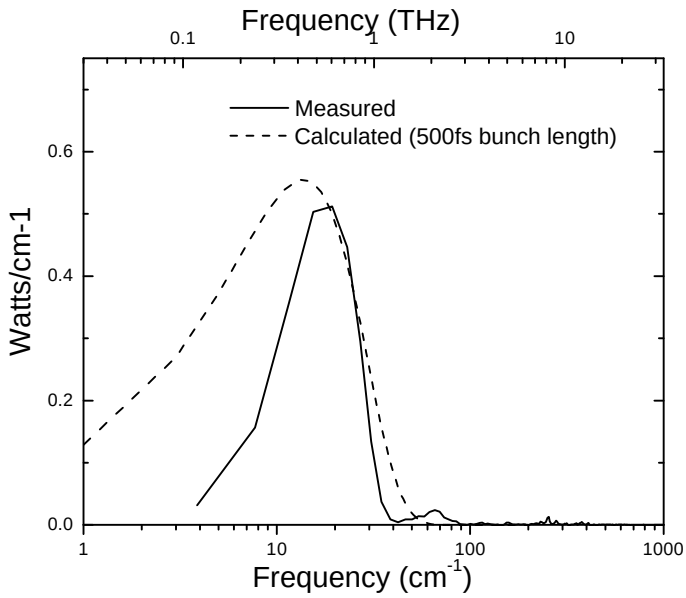

Fig. 3. Comparison between measured (solid line) and calculated (dashed line) THz spectral intensity.

switching mirror allowed a remote choice of source, namely the THz light from the accelerator, or a T=1300 K thermal reference source.

For the spectroscopy experiments, the analysis and detection system did not have sufficient dynamic range to cover the 7 decades in power difference between the 2 sources. We chose to make measurements at 584 kHz, instead of 37.4 MHz, and at a charge per bunch of 34 pC instead of the maximum of 100 pC, thereby reducing the THz power by a factor of $(37 \times 10^6) / (584 \times 10^3) \times (100/34)^2$, or approximately 550.

We show the results of the measurements along with a calculated curve for a bunch length of 500 fs in Fig. 3. We have scaled the data to fit the theory on the basis of the absolute power measurements. The spectral onset of the super-radiant enhancement is clearly seen, and the onset shape is also seen to match closely the theoretical predictions. Note that the discrepancy on the lower frequency side is due to diffraction effects.

We have another reference point for determining the absolute power since we were able to switch sources from the THz emission port to a 1300 K thermal source (the spectrometer's standard globar source). At a frequency of 12 cm^{-1} we obtained a ratio of intensity from the THz source to that of the globar of 2×10^4. To compare with the calculation, we multiply the THz source results by the reduction factor of 550, as discussed earlier. This implies a measured advantage of the JLab THz source over the globar of 10^7. The calculation predicts an enhancement of $(0.6 / 6 \times 10^{-8}) = 10^7$. While there is apparent agreement, these simple arguments have ignored diffraction and other effects on the detection efficiency of both sources. However, the result does indeed affirm the THz power.

We additionally observed the expected quadratic dependence of the coherent THz intensity on the number of electrons in the bunch, and the intensity ratio for the horizontal to vertical polarization components was measured to be 5. The expected polarization ratio for 30 cm^{-1} and 60 mrad is about 6, so we consider this to be good agreement.

CONCLUSIONS

We have demonstrated that the short bunches which circulate in energy recovery electron circulating rings with sub-picosecond electron bunch lengths yield broadband high brightness THz radiation with close to 1 W/cm^{-1} of average power into the diffraction limit and peak powers about 10^4 times higher than this.

This work was supported primarily by the U.S. Dept. of Energy under contracts DE-AC02-98CH10886 (Brookhaven National Laboratory), DE-AC03-76SF00098 (Lawrence Berkeley National Laboratory) and DE-AC05-84-ER40150 (Thomas Jefferson Natiional Accelerator Laboratory). The JLab FEL is supported by the Office of Naval Research, the Commonwealth of Virginia and the Laser Processing Consortium.

Principal investigator: Michael C. Martin, Advanced Light Source, Lawrence Berkeley National Laboratory. Email: MCMartin@lbl.gov. Telephone: 510-495-2231.

New IR microscope and bench installed at BL1.4

Michael C. Martin[a], Hoi-Ying N. Holman[b], and Wayne R. McKinney[a]
[a] Advanced Light Source Division, Lawrence Berkeley National Laboratory, Berkeley, CA 94720
[b] Center for Environmental Biotechnology, Lawrence Berkeley National Laboratory, Berkeley, CA 94720

1. INTRODUCTION

New infrared spectromicroscopy equipment was purchased for and installed on the ALS infrared beamlines on beam port 1.4. It includes the latest step-scan capable FTIR bench and an infinity corrected infrared microscope which will allow for a number of new sample visualization methods. This equipment was purchased with funding from the DOE Office of Biological and Environmental Research (OBER) with the express purpose to develop biomedical and biological applications of synchrotron-based infrared spectromicroscopy.

2. EQUIPMENT

The new spectromicroscopy equipment includes a Thermo Nicolet Nexus 870 step- and rapid-scan FTIR bench, and a Thermo Spectra-Tech Continuum IR microscope, photographed below. The IR microscope includes two IR detectors, a wide-band MCT and a fast (20 ns) TRS MCT for time-resolved experiments. A fast digitizer (up to 100MHz) compliments the TRS MCT detector. The synchrotron beam coupled into the IR microscope continues to have a diffraction-limited spot size, thereby attaining a 200-fold increase in signal from small (3 – 10 micron) sample spot compared to a conventional thermal IR source. The infinity-corrected microscope optics allow for a number of additional sample visualization accessories which can help the user identify the important location within their sample for micro-IR analysis:

- Visual and IR polarizers
- Dark-field illumination
- DIC (Differential Interference Contrast) optics
- UV Fluorescence

An example of DIC optics enhancing a micrograph of human cheek cells is shown in the photograph to the right. The DIC technique provides a psuedo-3D effect, enhancing the contrast between different thicknesses of an otherwise clear sample. In the image to the right, one can make out the nuclei of the cells (thicker bump near the middle of each cell), whereas this would be difficult using conventional illumination.

This new instrument will aide in user scientific research across many fields. For example, the study of individual living cells, toxic contaminants, bioremediation, protein microcrystals, rhizoids, and forensic evidence will all be enhanced by the additional capabilities of this new SR-FTIR spectromicroscopy system.

ACKNOWLEDGEMENTS

This research was supported by the Office of Science, Office of Biological and Environmental Research, Medical Science Division and the Office of Science, Office of Basic Energy Sciences, Materials Sciences Division, of the U.S. Department of Energy under Contract No. DE-AC03-76SF00098 at Lawrence Berkeley National Laboratory.

Principal investigator: Michael C. Martin, Advanced Light Source Division, LBNL, 510-495-2231, MCMartin@lbl.gov

Status of the 5.3.2 bend magnet polymer STXM

David Kilcoyne[1], Harald Ade[1], Tolek Tyliszczak[2], A. Peter Hitchcock[2], Adam P. Hitchcock[2], E.G. Rightor[3], G.E. Mitchell[3], Mike Kritscher[4], Tony Warwick[4], Keith Franck[4], Erik Anderson[5]

[1]Dept. of Physics, North Carolina State University, Raleigh, NC 27695
[2]BIMR, McMaster University, Hamilton, ON, Canada L8S 4M1
[3]Dow Chemical, 1897 Bldg, Midland, MI 48667
[4]Advanced Light Source, Berkeley Lab, Berkeley, CA 94720
[5]Center for X-ray Optics, Berkeley Lab, Berkeley, CA 94720

INTRODUCTION

Over the past three years a qualitatively new design of Scanning Transmission X-ray Microscope (STXM) has been conceived, built and commissioned at beamline 5.3.2 at the ALS. A dramatic improvement in performance has been achieved by introducing laser interferometry to control the positioning of microscope components with an accuracy consistent with the optical resolution of the instrument, currently about 40 nm. The interferometer is a great advance over previous systems such as the old BL7.0 STXM at the ALS and the Stony Brook STXM at the NSLS. In the latter instruments, one could image at a fixed photon energy with a spatial resolution close to the diffraction limit of the zone plate utilized, but it was not possible to change the photon energy while maintaining the focused X-ray spot on the same place on a sample, or to image at successive energies over the same x-y frame. Hence, the spatial resolution was effectively degraded for chemical analysis. Over a typical C 1s NEXAFS scan from 280 to 320 eV the focal length changes by up to 300 μm, requiring displacement of the zone plate along the X-ray beam by this amount while simultaneously maintaining the lateral position of the zone plate relative to the sample with <20 nm precision. Mechanical systems achieving the required linearity of $>10^4$ are exceptional, and indeed, the experience at both the ALS and NSLS microscopes has been that spatial resolution in point spectral mode is rarely better than 200 nm and that one needs to use software to correct for image-to-image misalignment, with concomitant residual resolution degradation.

EXPERIMENTAL

The solution that has been developed by a team from several institutions, adopted for both the 5.3.2 STXM and the 7.0 upgrade with somewhat different implementation, is to introduce a 2-d laser interferometer which continuously monitors the relative (x,y) position of the zone plate and the sample (see **Fig 1**). In the 5.3.2 STXM the interferometer is used as part of the feedback control loop for the PI piezo fast scan stage which is used to position and scan the sample when making images. This system provides stability of

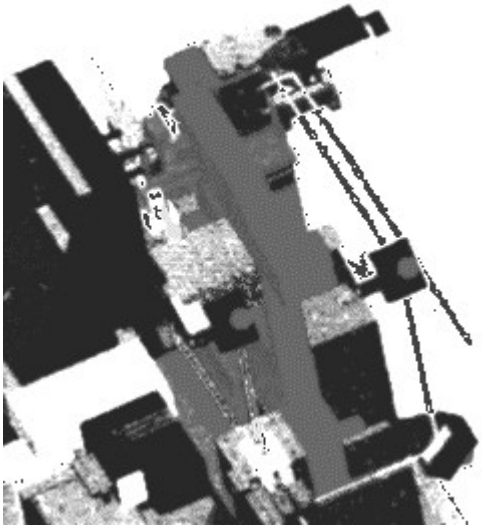

Fig. 1. View of the sample and zone plate stage region of the 5.3.2 STXM showing the paths of the laser beams used for 2-d interferometric control of relative position of the sample and the focused light.

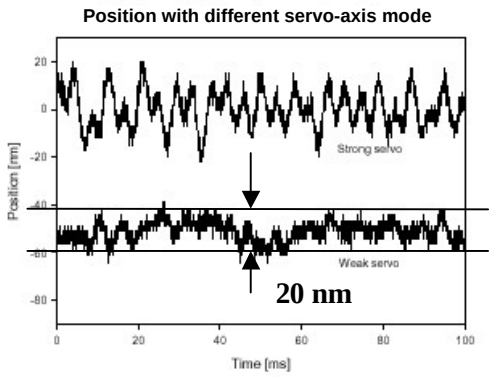

Fig. 2. Tests of positional stability over time of the sample position when under interferometric control (Tyliszczak, Feb-01)

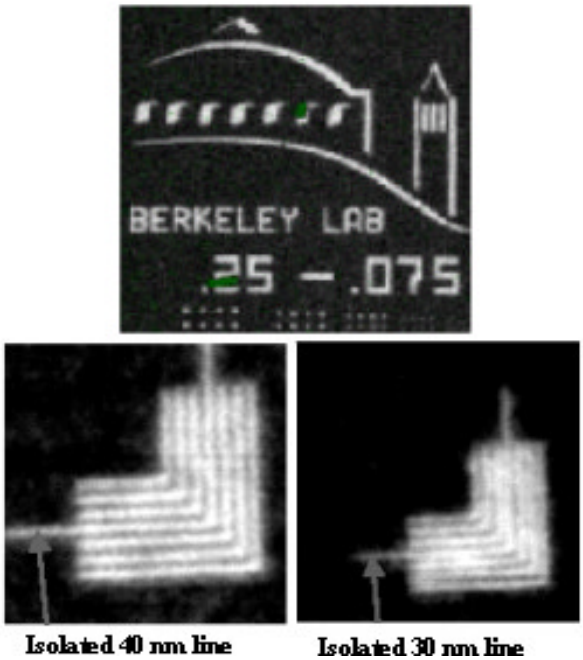

Fig. 3. Resolution tests using 1:1 Au lines on a silicon nitride substrate. The 40 nm pattern is fully resolved; the 30 nm pattern is partially resolved. (Each pattern consists of alternating lines and spaces of 30 or 40 nm). Zone plate and test pattern prepared by Erik Anderson *et al.* (CXRO, LBNL)

better than 20 nm with response times up to 100 Hz (see **Fig 2**) and thus it not only eliminates energy-to-energy image position errors, but also helps to desensitize the microscope to vibrational or other environmental noise.

With this mechanical/optical/control system, accompanied by advanced control and acquisition software, as well as excellent performance of the 5.3.2 spherical grating monochromator beamline [1], the 5.3.2 STXM is able to achieve diffraction limited spatial resolution. The images of a Au test pattern (**Fig 3**) indicate a spatial resolution of better than 40 nm, which is the theoretical diffraction limited resolution of the zone plate used. More significantly for analytical applications, the interferometry allows the 5.3.2 microscope to retain image registry at all photon energies. As an example of the level of positional stability achieved with the interferometry system, **Fig. 4** compares a linescan data set acquired at BL 5.3.2 in August 2001 on a polyurethane sample containing nanoscale filler particle with a data set on a similar sample recorded over a similar spatial and photon energy range, acquired with the old ALS beamline 7.0 STXM. In each case the raw data - position along line versus photon energy - is plotted. Clearly the ability to determine the NEXAFS spectra at high spatial resolution is greatly enhanced by the improved performance of the 5.3.2 STXM.

Further work on both the beamline and the mechanical and controls system has further increased stability and reliability of the 5.3.2 STXM [2] relative to its performance when these test measurements were performed.

REFERENCES

1. T. Warwick, *et al.* J. Synchrotron Rad. Submitted Jan 2002.
2. A.L.D. Kilcoyne *et al.* J. Synchrotron Rad. In preparation

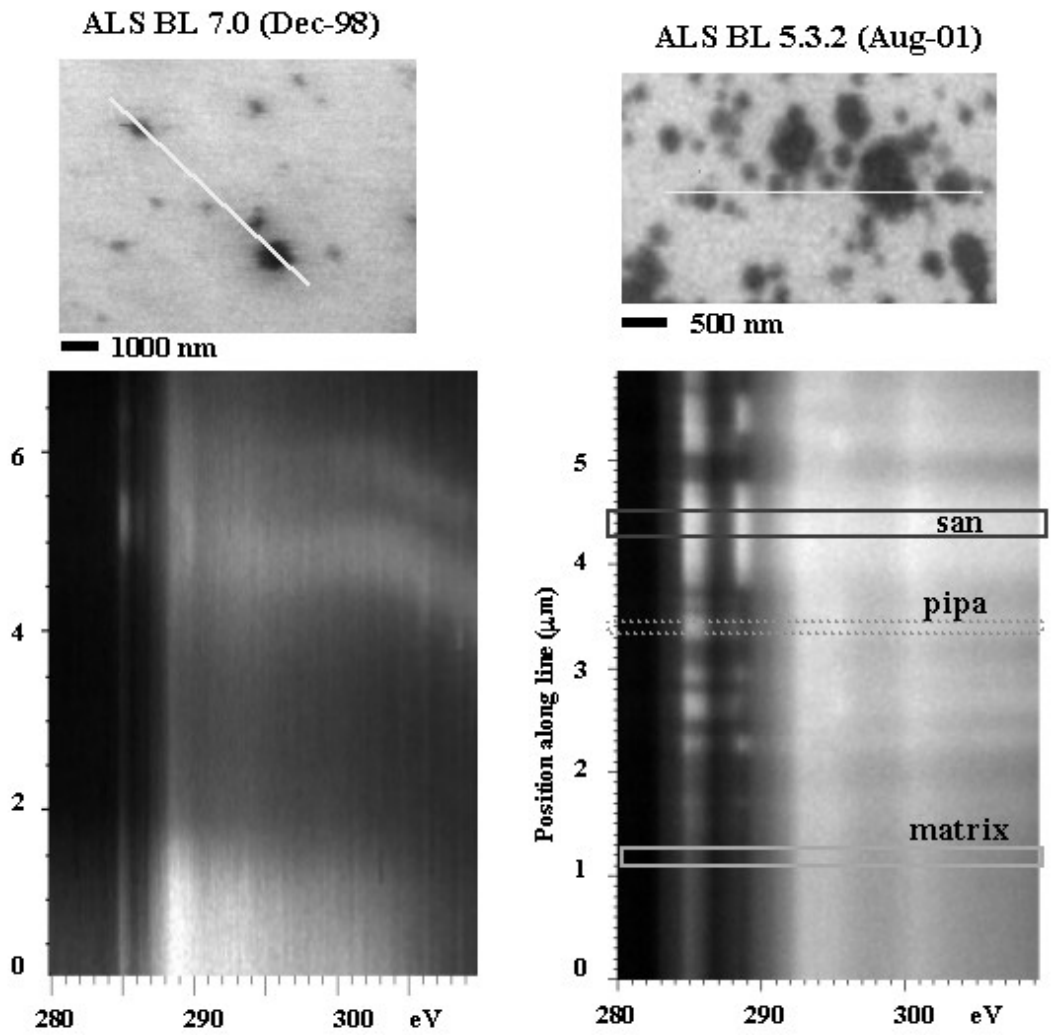

Fig. 4.
the old BL7.0 STXM and the new 5.3.2 STXM using data from filler particles (pipa) in a low-water polyurethane sample. The two lower 'images' plot 'linescans spectra' measured with each instrument. The display shows photon energy horizontally and position vertically - successive horizontal lines are the spectrum at pixels nominally along the line indicated in the true OD image of the samples displayed on the top (BL7.0: pipa only; BL5.3.2: pipa and san). The waviness of the signal in the horizontal direction in the left hand linescan is caused by drift of the X-ray spot on the sample due to mechanical limitations. In contrast, in the right hand linescan, there is negligible waviness in the horizontal direction. This is because the interferometric control in the 5.3.2 STXM provides precise zone plate - sample positioning at all photon energies. It also provides significant dynamic compensation for vibrations. Vibrations were present in the old 7.0 STXM and degraded its spatial resolution.

Capital costs for the beamline were provided by the ALS. Development costs for the STXM instrument were provided by DOE (DE-FG02-89ER60858), NSF (NSF DMR-9975694), the NSERC strategic program, Dow Chemical, and NCSU. The work of the McMaster group is supported by research and partnership grants from NSERC (Canada), the Canada Research Chair program (APH). The ALS is supported by the U.S. DOE, Office of Science.

Principal investigator: *Harald Ade*, NCSU, **harald_ade@ncsu.edu**. Ph: 919-515-1331

Status report on Beamline 10.3.2

Matthew Marcus
Lawrence Berkeley National Laboratory, Berkeley, CA 94729

Beamline 10.3.2 has had a varied history, starting as an optics-development beamline on which new techniques could be explored, then evolving into an X-ray microprobe beamline. In its latest incarnation, it's a hard X-ray microprobe beamline optimized for environmental studies, with μEXAFS and μSXRF capabilities. Two years ago, the optics were changed to allow more flux at the cost of a bigger, but adjustable, spot size. The beamline came up to full user operation in November, 2001 and is now fully booked. While most of the users have been looking at speciation of metals in earth materials, there have also been projects in archeometry, osteology and microbiology.

The beamline can deliver white or monochromatic beam in a spot ranging from 16x6μm (full flux) down to 5x4μm FWHM. The energy range is 3-17keV. The optical layout consists of a horizontally deflecting 1:1 toroid, focusing to a slit, followed by optics inside the hutch, consisting of a vertically collimating parabolic mirror, 4 crystal monochromator, horizontally focusing ellipse and a vertically refocusing parabolic mirror. The optical layout is shown in Figure 1.

The sample is carried on a an XY stage with 10nm steps, and fluorescence radiation is detected by a 7-element Ge detector. Fluorescence mapping is done in a continuous-scan fashion in which the stage moves at a constant speed. The detector electronics allows one to define spectral regions of interest (ROIs) in which counts are accumulated. At fixed distance intervals, these counts are loaded into successive locations in the internal memory of the detector electronics. Thus, a line scan is built up without the need to step and repeat for each point. Successive line scans result in a two-dimensional fluorescence map.

These maps may be used to choose points at which to do EXAFS. This combination of fluorescence mapping and EXAFS is very useful in deciphering the structures of complex, inhomogeneous systems. Also, we have recently acquired a CCD for powder diffraction. Once that is integrated into the system, we will have the uniquely powerful combination of μSXRF, μEXAFS and μXRD, all available on the same sample in the same run.

An example of a fluorescence map from Alain Manceau's work is shown in Figure 2. This illustration shows gray-scale maps of the same ferromanganese soil nodule taken in the 'light' of several different elements. One can see, for instance, that areas high in Mn are low in Fe, that Ca exists mostly in the form of isolated mineral grains, and that As is found where Fe is. Such information, backed up with detailed analysis of EXAFS spectra, can shed light on how trace elements are sequestered in the environment, and hence add scientific rationale to the process of soil remediation.

For the April shutdown, we are planning to replace the 4-bounce monochromator with a 2-bounce, constant-height unit, which will yield a 3-10x flux improvement. Also, we plan to implement automatic mirror tuning, which will result in smaller spots and greater reliability. We now also have a Bruker SMART 6000 diffraction camera for the end station, and this will be fitted by summer '02. This will allow a range of diffraction experiments to be conducted, and will offer a similar capability to beamline 7.3.3, but with the addition of XAS. We are also examining the improvement in performance that would result from moving the system to a superbend. Improvements range from around 10 at 12 keV to nearly 100 at 20 keV, and would allow a much wider range of elements to be studied.

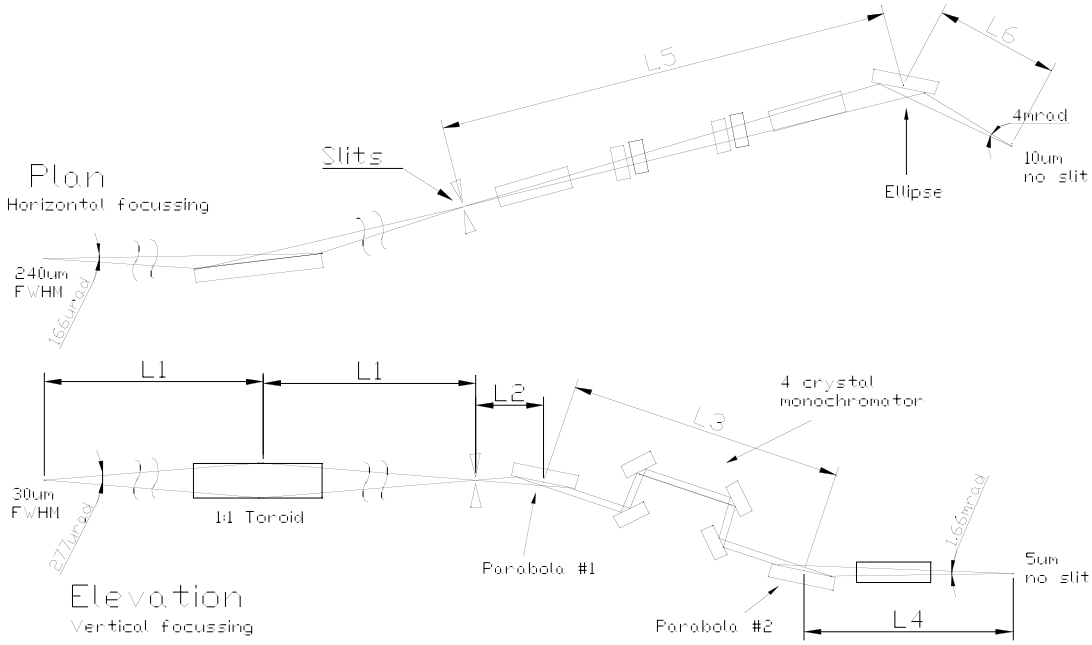

Figure 1. Optical layout. The dimensions L1..L6 and mirror types are as follows:

L1 = 14.75m	*Mirror*	*Type*	*Active area*
L2 = 1.44m	*M1*	*1:1 toroid*	*612 x 4.63mm*
L3 = 0.820m	*M2*	*V parabola*	*100 x 0.23mm*
L4 = 0.26m	*M3*	*V parabola*	*100 x 0.37mm*
L5 = 2.4m	*M4*	*H ellipse*	*100 x 0.66 mm*
L6 = 0.12m			

Mirror grazing angles = 4 mrads (coating = 8nm Rh on 20nm Pt on 5nm Cr)

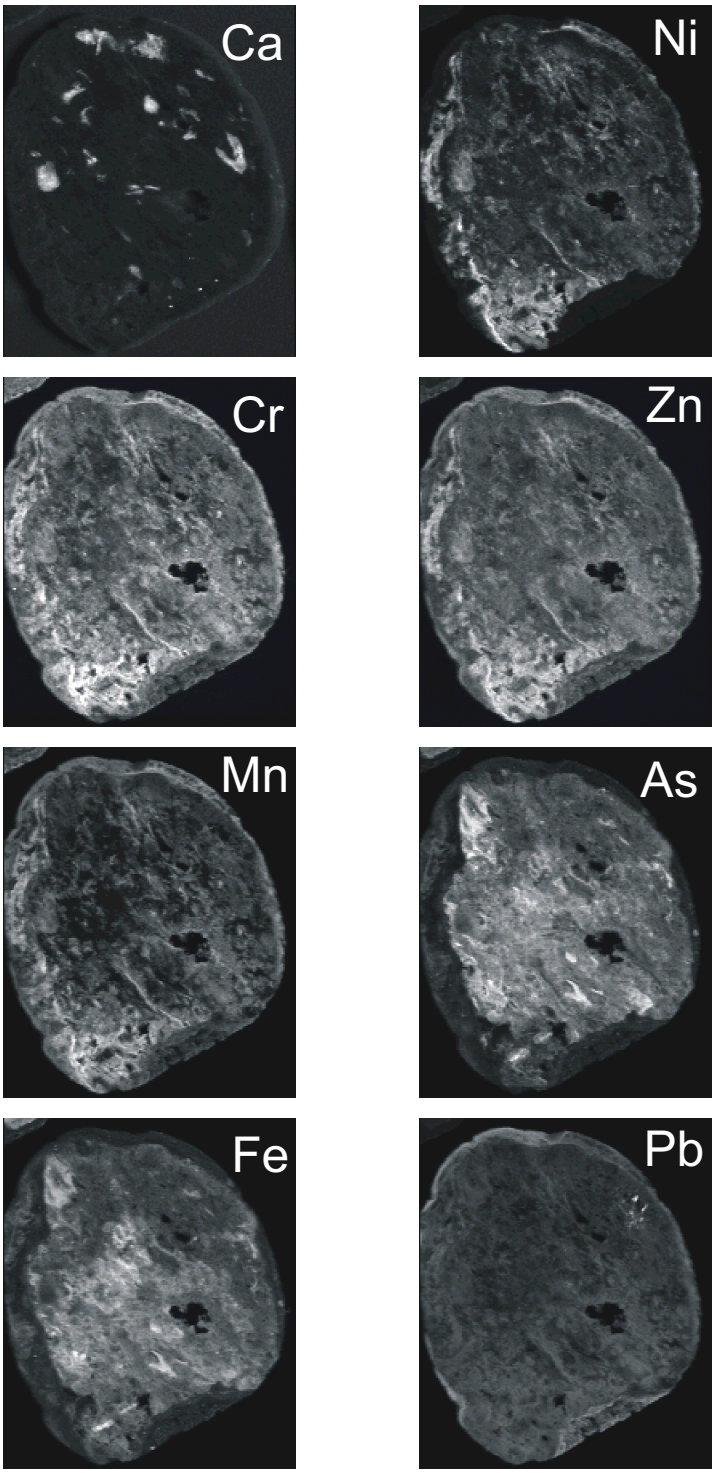

Figure 2. Elemental maps of a ferromanganese nodule. The As and Pb maps were taken below and above the Pb L_{III} edge, respectively, in order to separate the signals from these two elements.

This work was funded by the U.S. Department of Energy, Office of Science, Office of Basic Energy Sciences, Materials Sciences Division.

Contact person: Matthew A. Marcus, Advanced Light Source, Lawrence Berkeley National Laboratory.
Telephone: (510) 486-7604. Email: MAMarcus@lbl.gov.

Suite of Three Protein Crystallography Beamlines with Single Superconducting Bend Magnet as the source.

A.A.MacDowell[1], D.Cambie[2], D.Plate[2], R.Duarte[2], N.Kelez[2], H.A.Padmore[1], M.Howells[1], R.Celestre[1], E.Domning[1], J.Holton[3], C.Cork[3], T.Earnest[3], J.Dickert[3], G.Meigs[3], J.Krupnick[1], T.Alber[4], S.Berger[4].

[1]Advanced Light Source Division, Ernest Orlando Lawrence Berkeley National Laboratory, University of California, Berkeley, California 94720, USA
[2]Engineering Division, Ernest Orlando Lawrence Berkeley National Laboratory, University of California, Berkeley, California 94720, USA
[3]Physical Biosciences Division, Ernest Orlando Lawrence Berkeley National Laboratory, University of California, Berkeley, California 94720, USA
[4] Dept. of Molecular and Cell Biology, 229 Stanley Hall, University of California, Berkeley, California, 94720, USA

INTRODUCTION

At synchrotrons around the world Protein Crystallography beamlines are being built at a rapid pace as it has been realized that this technique can rapidly elucidate protein structures, which can provide one of the foundation blocks for the understanding of life. Many Protein Crystallography beamlines are required as there are many tens of thousands of protein structures to solve. Here at the Advanced Light Source (ALS), a consortium from the Universities of Berkeley and San Francisco have constructed beamline 8.3.1, quickly followed by the Howard Hughes Medical Institute funding the construction of two more identical beamlines (8.2.1 and 8.2.2). All three beamlines are adjacent and use as a source one of the three newly installed 5 Tesla single pole Superconducting-bending magnets. Beamline 8.3.1 is in operation and the other 2 beamlines are finalizing the commissioning process. This document will briefly describe these beamlines and their initial performance.

BEAMLINE DESIGN

Initial work was carried out in 1998 by the University of Berkeley (UCB) group on the test beamline 7.3.3 to determine the feasibility of carrying out Protein Crystallography on regular ALS bending magnets. Complete multiple anomalous dispersive data sets were collected to 1.9Å resolution in ~ 10hours on the non- optimized test beamline [1]. By optimizing the beamline and switching from a regular warm magnet dipole source to a 5 Tesla Superconducting dipole source [2], it would be expected that scan times would drop to ~ 1hour. Speed is increasingly becoming very important for the Protein Crystallography process both due to the large number of protein structures to be solved and the requirement to scan for good samples amongst the many poor ones during the iteration of crystallization procedures.

The simplistic basis for the beamline design was to put as many 6-16 KeV photons through a 100μm diameter pinhole as possible consistent with reasonable cost and robust performance. The optimized beamline design schematic is shown in figure 1. 1.5mrad (h) x 0.5mrad (v) of radiation is accepted by the nickel-plated water-cooled invar mirror (M1), 6.5m from the source. It is shaped into a parabolic cylinder by means of a bending mechanism. Parallel light in the vertical plane is directed into a water-cooled double crystal monochromator (Kohzu

Co.) 18m from the source. The exiting monochromatic light is focused by a toroidal mirror (M2) (21.53m) onto the sample in the hutch with a horizontal demagnification of 2. The end stations are of the mini-hutch type allowing for changing samples by reaching through a sliding door. Ray tracing indicated that using a dipole source size of 230µm (h) x 23µm (v) fwhm resulted in a focused spot size of 150µm (h) x 67µm (v) fwhm with a divergence of 3mrad (h) x 0.33mrad (v).

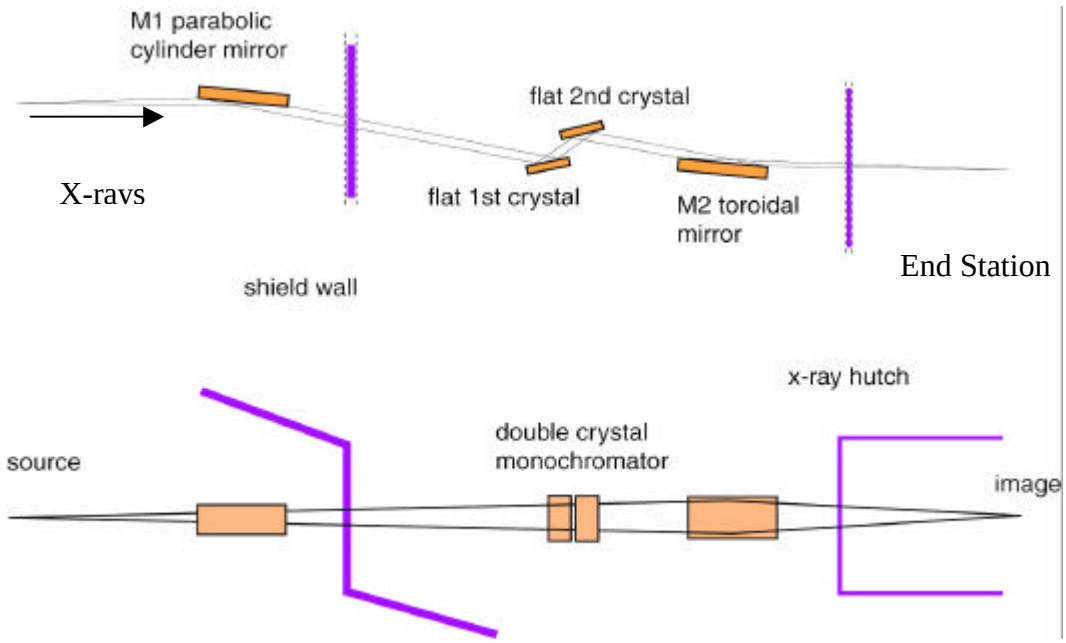

Figure 1. Schematic layout of the new Protein Crystallography Beamlines with a Superbend dipole magnet source. Mirror grazing angles are 4.5mrads.

BEAMLINE PERFORMANCE

The focus spot size at the sample has been measured on the 3 beamlines as ranging from 150µm (h) x 120-160µm (v). This is slightly higher in the vertical than expected and is most likely due to figure and roughness problems that arose during the manufacture of the M1 mirrors. New ones are currently being fabricated. The flux through the 100um pinhole is calculated as 2 x 10^{11} hυ/sec at 12.4KeV (ALS =400mA), but the actual flux measured is less being in the range of 4-8 x 10^{10} hυ/sec at) for the 3 beamlines. This too is expected to improve when the new M1 mirrors are installed. The x-ray convergence angles onto the sample were 1.5mrad (h) x 0.33mrad (v). This is still a very respectable flux and very comparable to the 5.0.2 Protein Crystallography beamline, which uses a 38-pole 2.1 Tesla wiggler magnet insertion device. This is a high power, low brightness source and yields a sample flux of 7x10^{10} hυ/sec at 12.4KeV for the same conditions as used on the Superbend beamlines. This confirms the original concept that the high brightness low power Superbend dipole source can compete with high power low brightness insertion devices for selected applications.

Beamline 8.3.1 has been operational for 2-3 months and has solved 17 structures. Beamlines 8.2.1 and 8.2.2 are undergoing the final commissioning.

REFERENCES

1. T. Alber, J.M. Holton, J.Plecs, R. Rose, A.A.MacDowell, R.S. Celestre, H.A. Padmore, The practicality of an ALS bend magnet as the x-ray source for solving structural biology problems. Advanced Light Source Activity Report, Abstracts 1998
2. Advanced Light Source Activity Report 2001, Facilities Report Section.

This work was supported by the Director, Office of Energy Research, Office of Basic Energy Sciences, and Materials Science Division, of the U.S. Department of Energy under Contract No. DE-AC03-76SF00098.

Principal investigator: Alastair MacDowell, Advanced Light Source, Ernest Orlando Lawrence Berkeley National Laboratory. Email: aamacdowell@lbl.gov. Telephone: 510-486-4276.

The use of micro-FTIR to characterize soil minerals and Boron adsorption

S. Pittiglio and H.E. Doner
Ecosystem Sciences Division – Environmental Science, Policy and Management,
University of California, Berkeley, California 94720-3110, USA

INTRODUCTION

This study was carried out in an effort to obtain direct structural information of adsorbed boron on the solid surfaces of soil material (clays and oxides). It is necessary to understand the relationship between trace elements and clays at a molecular level to describe and predict interfacial processes controlling trace element retention and release in soils. Our goals for this last proposal period were: 1) to build a spectral library of clay minerals, oxides and boron containing minerals commonly found in California soils. This library would be used to conjunction with x-ray diffraction (XRD) data to determine if micro-Fourier transformed infrared spectroscopy (μ-FTIR) is an appropriate method for identifying clay minerals in soil matrices. 2) Determine which minerals in our spectral library are applicable for studying boron (B) adsorption. Previous studies have found that amorphous $Fe(OH)_3$ and amorphous $Al(OH)_3$ are both suitable for B adsorption studies [1]. In past work we found a clear spectral differentiation between gibbsite that had been untreated with B and B treated could be detected [2]. These differences are due to specific adsorption of B onto the mineral surfaces. 3) Use a benchtop attenuated total reflectance-Fourier transformed infrared spectroscopy (ATR-FTIR) to examine the coordination of boron adsorption on magnesium hydroxide ($Mg(OH)_2$).

B has been identified as one of the major trace elements responsible for soil degradation in irrigated areas of the world [3]. Although B is an essential micronutrient for plants, it can also be toxic at concentrations greater than 1 mg L^{-1} [4]. In arid and semi-arid regions of the world, where soils are subject to high evapotranspiration rates and poor water quality, they can become enriched in B, becoming an important factor in leaving large areas in the landscape devoid of vegetation.

Boron biogeochemistry is a major factor in managing land reclamation in arid and semi-arid ecosystems. A key factor limiting progress in land management is understanding the processes involved in the retention and slow release of B from the soil inorganic and organic solid-phase. Combining μ-FTIR with ATR-FTIR and XRD, we aim to characterize the composition of the soil matrix and possibly the form and location of B in the soil matrix.

METHODS

Peds (intact pieces of soil) were collected from the Panoche soil series in Fresno County, CA. The Panoche soils are known to be high in B. Yellow and brown deposits were noted throughout the soil profile. The soil peds were air dried at 35^0C and impregnated with LR White high grade resin under a vacuum in order to retain soil aggregate structure. The resin was hardened by heating samples at 60^0C for 48 hours. The hardened samples were cut into thin sections (0.1-0.2 cm thick) using a diamond edged saw and polished to ensure a smooth surface. The thin sections were then analyzed using μ-FTIR on Beamline 1.4.3. The clay-sized fraction of this soils was also analyzed by XRD to determine clay mineralogy.

Minerals containing B, clay minerals and oxides were obtained for the spectral library. These minerals were analyzed by benchtop FTIR, μ-FTIR and XRD. This provided us with

samples of known characteristics for comparison and were used to create a searchable library in Omnic 5.1.

Boron was also adsorbed onto brucite ($Mg(OH)_2$) at varying pH's. Samples of 0.3 g MgO were added to 50 mL polypropylene centrifuge tubes containing 25 mL's of 20 ppm B solution, and were shaken for 24 hrs. The suspension pH was adjusted to the desired levels with 1.0 M HCl or NaOH. The supernatant solutions were separated by centrifugation, filtered through a 0.1 mm filter and analyzed for B concentration by inductively couples plasma-atomic emission spectrometry (ICP-AES). The amount of B adsorbed was calculated as the difference between the total B added and the B that remained in the aqueous solution. The solid material remaining was air dried at room temperature and analyzed by ATR-FTIR and XRD.

RESULTS AND DISCUSSION

μ-FTIR seems to be an appropriate method for the qualitative identification of clay minerals. The spectral library of clay minerals created in Omnic 5.1 was able to correctly identify the clays (originally determined by XRD) in the Panoche soil we collected. The μ-FTIR was useful because we were able to determine the clay mineralogy of specific aggregates in our soil thick-sections. Figure 1 shows the results of a search on the soil matrix. The XRD work done on bulk samples of the Panoche soil gave the same results as the μ-FTIR. The μ-FTIR provides great advantages over common XRD procedures for determining the clay mineralogy which only considers homogenized bulk samples. The drawbacks to this method were that the signal from the hardening resin can interfere with the signal from the samples. Subtracting the resin signal did not remove the interference in all cases.

We found that many of the minerals commonly found in soils are inappropriate for studying B adsorption using FTIR. This is due to the fact that many clay minerals have adsorption bands in the same locations as B adsorption bands. The criteria for selecting minerals appropriate for this study was an absence of bands in the 1600-1150 cm^{-1} and the 1100-850 cm^{-1} region. Bands in the 1600-1150 cm^{-1} region make it difficult to detect trigonally coordinated B ($B(OH)_3$), and bands in the 1100-850 cm^{-1} region make it difficult to detect tetrahedrally coordinated B ($B(OH)_4^-$). Therefore, this criteria excludes most clay minerals from B adsorption studies using FTIR, since most clays have adsorption bands in the 1100-850 cm^{-1} region, due to the Si-O asymmetric stretching mode.

We found that $Mg(OH)_2$ may also be promising for B adsorption studies. Magnesium minerals have previously been identified as having appreciable boron-sorption capacities [5]. Since this discovery, no research has investigated this phenomenon in detail.

Samples of $Mg(OH)_2$ with 1046 mg B kg^{-1} sorbed were analyzed using ATR-FTIR. We could not identify any significant spectral differences between the B treated and untreated $Mg(OH)_2$. It is possible that the concentration is too low for IR detection or that B is not specifically adsorbing. Another explanation might be that the adsorption bands for trigonal B were masked by a broad adsorption band for carbonate at 1420 cm^{-1}. These solid phase carbonates may have formed in solution and adsorbed, or they could be carbonates formed at the surface of the mineral.

Figure 1 – Results of the Spectal Search for the Panoche Soil

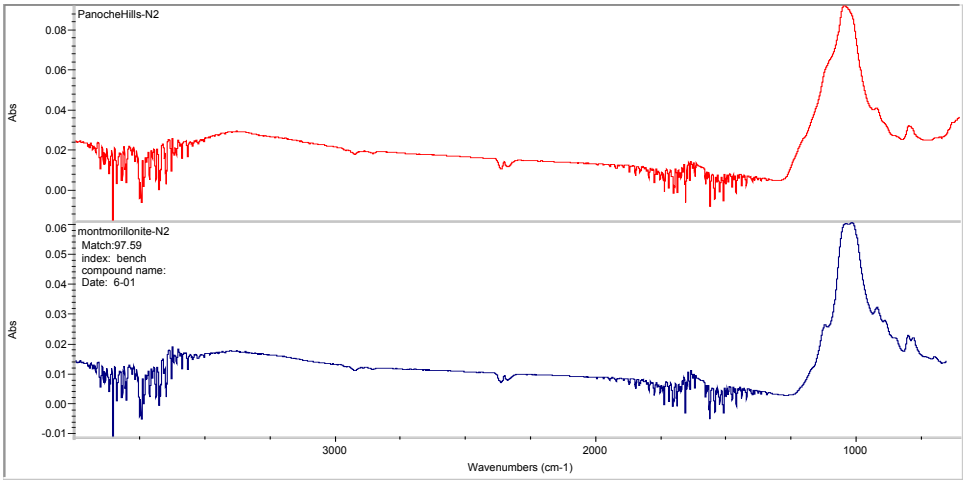

Figure 1 – The top IR spectrum is from the Panoche Soil Series and the bottom spectrum shows the library search results. This match shows that the Panoche soil is predominantly montmorillonite clay.

The μ-FTIR technique has many clear advantages for investigating chemical processes in natural microenvironments as exists in soils. Although our results over that past year were inconclusive, the development of a spectral library will greatly enhance the application of this technique. As an example, given the economic significance of B toxicity in many irrigated systems of the world, a greater understanding of the role of magnesium minerals in controlling the distribution of B in natural systems is crucial for predicting availability, potential toxicity problems, and is essential for evaluating how B rich soils should be managed.

LITERATURE CITED

[1]Chunming Su and Donald L. Suarez, "Coordination of adsorbed boron: An FTIR spectroscopic study," Environmental Science and Technology **29** (2), 302-311 (1995).
[2]P. Fox, H.E. Doner, and S. Pittiglio, "Micro-scale distibution of trace elements in a high boron soil from Kern County, California,", (2001).
[3]J. Hren and H. R. Feltz, "Effects of irrigation on the environment of selected areas of the Western United States and implications to world population growth and food production," Journal of Environmental Management **52** (4), 353-360 (1998).
[4]F. T. Bingham, A.W. Marsh, R. Branson et al., "Reclamation of salt-affected high boron soils in western Kern County," Hilgardia **41** (8), 195-211 (1972).
[5]J. D. Rhoades, R. D. Ingvalson, and J. T. Hatcher, "Adsorption of boron by ferromagnesian minerals and magnesium hydroxide," Soil Science Society of America Journal **34**, 938-941 (1970).

ACKNOWLEDGMENTS

We appreciate the assistance of Michael Martin of the ALS.

This work was supported by USDA regional research project CA-B*-ECO-5515-RR and USDA Hatch project CA-B*-ECO-6135-H

Principal investigator: Harvey Doner, Ecosystem Sciences Division – ESPM, University of California, Berkeley. Email: doner@nature.berkeley.edu. Telephone: 510-642-4148